DIAGNOSTIC NUCLEAR MEDICINE

Lesion Detection with Single-Photon Emission Computed Tomography (SPECT) Compared with Conventional Imaging

Ronald J. Jaszczak, Frank R. Whitehead, Chun Bin Lim, and R. Edward Coleman

Duke University Medical Center, Durham, North Carolina and Siemens Gammasonics, Inc., Des Plaines, Illinois

We have evaluated analytically and experimentally the effectiveness of both conventional nuclear medicine imaging and single-photon emission computed tomography (SPECT) imaging to detect small photon-deficient areas (approximately the size of the system's resolution) within a relatively uniform background. The experimental model is based on the Tc-99m sulfur colloid study of the liver. The experimental data were obtained from a liver phantom containing two small photon deficient areas, nominally 1 and 1.5 cm in diameter. The liver phantom was placed in a water-filled Alderson body phantom and scanned with the cold defects located both centrally and peripherally. Lesion image contrast for both conventional and SPECT imaging is proportional to the lesion uptake ratio and is degraded by the system's finite spatial resolution and Compton-scattered photons. However, for conventional imaging the contrast is significantly degraded by the effect of radionuclide superposition (as modified by attenuation), while for SPECT imaging the contrast is essentially independent of these effects. This results in a significant increase in lesion-to-background contrast with SPECT as compared with conventional imaging. The measured SPECT image contrasts for the 1- and 1.5-cm areas of low uptake averaged more than five times the measured image contrasts for the conventional system.

J Nucl Med 23: 97–102, 1982

The imaging characteristics of conventional scintillation cameras have been analyzed previously by Whitehead (*1*) and more recently by Shosa and Kaufman (*2*) using a linear systems model. The linear systems model has recently been applied by Jaszczak et al. (*3*) to the investigation of the capability of single-photon emission computed tomography (SPECT) with complete angular sampling to quantitate radionuclide distributions and detect lesions. The object of this report is to evaluate this model experimentally as applied to the imaging of small (1–2 cm) defects containing no radionuclide activity and surrounded by a relatively uniform background. This model is based on the Tc-99m sulfur colloid study of the liver.

Received July 30, 1981; revision accepted Sep. 25, 1981.

For reprints contact: Ronald J. Jaszczak, PhD, P.O. Box 3949, Duke University Medical Center, Durham, NC 27710.

METHODS AND MATERIALS

Theory. If an imaging system is linear and generates artifact-free images, there are two principal characteristics of the image that determine whether an observer will detect the presence of a small defect or "lesion," approximately the size of the system's resolution, in a relatively uniform background. First, the magnitude of the lesion's image contrast defined as

$$C_{image} = \frac{\text{counts/pixel}_{(lesion)} - \text{counts/pixel}_{(background)}}{\text{counts/pixel}_{(background)}} \quad (1)$$

must be greater than some factor k times the fractional

rms noise level:

$$|C_{image}| > k \frac{\text{rms noise level}}{\text{background level}}. \quad (2)$$

In other words, the *signal-to-noise* level must be greater than k. The value of k is based on statistical considerations, and is so chosen as to keep the probabilities of false positives and false negatives below a certain level. For a nuclear medicine image consisting of approximately 1000 resolution elements, the value of k should be between 4 and 5, assuming one is interested in detecting objects close to the size of a resolution element (*4*).

The second principal consideration is that the displayed lesion contrast must be greater than the visual threshold of the observer:

$$|C_{displayed}| > [\text{visual threshold of observer}]. \quad (3)$$

For example, using conventional nuclear medicine imaging techniques with film as the recording medium, the density difference must be greater than approximately 0.07 for spherical lesions to be detected in a uniform background.

Linear systems analysis has been applied to the situation where there is a spherical lesion in a uniform background, with an uptake ratio, or object contrast, defined as

$$C_{object} = (Q_s - Q_b)/Q_b, \quad (4)$$

where Q_s is the concentration (μCi/cc) in the spherical lesion and Q_b is the concentration in the surrounding background. It is then found that, for conventional imaging, the object contrast is affected by (a) the system's finite spatial resolution, (b) the inclusion of Compton-scattered photons within the energy window, and (c) the superposition of overlying and underlying radionuclide activity, modified by the effects of attenuation. For this model of conventional imaging the image contrast may be estimated using the following relation (*1*):

$$C_{image} = [(Q_s - Q_b)/Q_b] \cdot CF \cdot \frac{1}{1+SF} \cdot \frac{D}{L} \cdot [\text{attenuation factor}], \quad (5)$$

where Q_s is the concentration in the spherical lesion, Q_b is the surrounding background concentration, CF is the contrast factor due to the finite spatial resolution of the system, SF is the scatter fraction, D is diameter of the spherical lesion, and L is the thickness of the background medium.

The attenuation factor is derived from:

$$\text{Attenuation factor} = \frac{e^{-\mu_p Z}}{[\sinh(\mu_b L/2)/(\mu_b \cdot L/2)]e^{-\mu_b L/2}}, \quad (6)$$

where μ_p is the "effective" primary-photon attenuation coefficient (0.15 cm^{-1}) for the sphere, μ_b is the "effective" photon attenuation coefficient (0.1 cm^{-1}) (value depends on system's energy window setting) for the background, and Z is the depth of the sphere.

The contrast factor CF is a function of the system's spatial resolution at the depth of the lesion, relative to lesion size, and is always less than unity (*1*). The scatter fraction SF is defined as the ratio of scattered to unscattered photons (*5*), and depends on the energy window used and the depth of the lesion. For SF we used an estimated constant value of 0.4 for the results presented below. This value is consistent with the theoretical simulation results presented by Dresser (*6*).

As with conventional nuclear medicine imaging systems [Eq. (5)], SPECT image contrast is proportional to the uptake ratio $(Q_s - Q_b)/Q_b$, and is degraded by the system's finite spatial resolution (CF_{avg}) and the inclusion of Compton-scattered photons $(1 + SF_{avg})^{-1}$. To a first approximation, however, SPECT image contrast is *not* degraded by superposition (D/L), and is *not* affected by photon attenuation, provided an appropriate compensation algorithm is used. Of course, attenuation does affect the fractional rms noise level of SPECT images. SPECT image contrast may be estimated using the following equation (*3*):

$$C_{image} = [(Q_s - Q_b)/Q_b] \cdot CF_{avg} \cdot (1 + SF_{avg})^{-1}, \quad (7)$$

where $(Q_s - Q_b)/Q_b$ is the object contrast or uptake ratio, CF_{avg} is the average contrast factor, and SF_{avg} is the average scatter fraction.

An equation that can be used to estimate the SPECT % rms noise of a uniform disc source surrounded by a nonradioactive attenuating medium has been presented by Jaszczak et al. (*3*). For SPECT imaging, averaged values are used for the contrast factor and the scatter fraction, since the object is viewed through a complete 360° angular range. The average contrast factor CF_{avg} can be estimated using measured SPECT system resolutions, measured lesion diameter, and tabulated data previously presented by Whitehead for conventional gamma cameras (*1*).

Imaging systems and techniques. Our complete-angular-sampling SPECT system (*3,7*) consists of dual large-field-of-view (LFOV) Anger detectors* mounted on a rotatable gantry, a 32-bit minicomputer,† and a microprocessor-controlled display station with image memory. The reconstruction is performed using a filtered backprojection algorithm with compensation for photon attenuation and variations of detector sensitivity (*8–10*). The spatial-frequency filter consists of a ramp filter with modifications to both high and low spatial frequencies (*3,8*). Data presented here were reconstructed using filter "2" (having a cutoff frequency equal to 1.6 cycles/cm) defined by Jaszczak et al. (*3*). Conventional gamma images were obtained by operating one of the

SPECT scintillation detectors without rotation. Total detected events corresponded approximately to the number of detected events obtained in a typical liver scan. High-resolution, low-energy, parallel-hole collimation was used for both imaging modalities.

Experimental results were obtained using a phantom (Fig. 1) consisting of a simulated liver with two nearly spherical defects containing photon-deficient water (uptake ratio = −1): one ~1 cm i.d. in the left lobe and the other ~1.5 cm. i.d. in the right lobe. Both had plastic walls ~1 mm thick. Technetium-99m was uniformly distributed in the simulated liver, which was then placed in a water-filled Alderson body phantom. Conventional and SPECT images were obtained with the defects located both centrally and peripherally within the simulated liver. For the 1.5-cm defect in the approximately 12-cm-thick right lobe, the distances from the center of the defect to the surface of the lobe were 6 and 1.3 cm for the central and peripheral locations, respectively. For the 1-cm defect within the 7-cm-thick left lobe, these distances were 3.5 and 0.7 cm. The anterior surface of the simulated liver was ~5 cm from the anterior surface of the body phantom. For conventional gamma-camera imaging, the collimator was placed in close proximity to the anterior surface of the phantom's body. For SPECT imaging, the radius of rotation was 19 cm, providing clearance for the detectors during rotation about the body phantom. A clinical SPECT liver scan, lasting 26 min and using low-energy, all-purpose (LEAP) collimators, which have triangular holes, results in approximately 1 million total counts for a complete set of 180 projections in a single transverse section 6.4 mm thick. The newly developed square-hole LEAP collimators should have approximately this same sensitivity but with resolution equivalent to that of a triangular-hole, high-resolution collimator. Since the former collimator was unavailable for our system, the images for this report were acquired using triangular-hole, high-resolution collimation and accumulating 1 million total counts per 6.4-mm-thick transverse section. The conventional images were obtained with the same collimator, and contained 1 million counts per view. A 15% energy window (130–150 keV) was used for both studies.

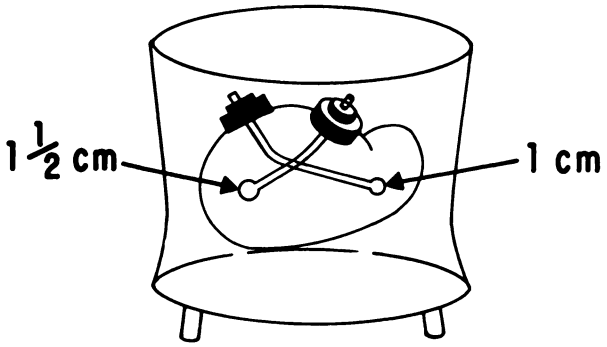

FIG. 1. Alderson body phantom with simulated liver containing photon-deficient regions with indicated inside diameters.

RESULTS

Table 1 shows the effects that the factors such as finite spatial resolution, Compton-scattered photons, superposition, and attenuation have on conventional and SPECT lesion contrasts. A larger estimated FWHM (1.3 cm) was used for the SPECT spatial resolution, compared with the 0.9 cm used for conventional gamma-camera imaging, since in SPECT the collimator surface is at an increased, average separation from the region of no radioactivity. Using the estimated values for the spatial resolutions at the depth of the defect and its approximate diameter, values of the contrast factor CF were determined using published data (*1*). Although the better spatial resolution of the conventional gamma camera results in less contrast degradation compared with SPECT systems using a circular orbit, the elimi-

TABLE 1. FACTORS AFFECTING LESION CONTRAST, ASSUMING A REGION OF NO RADIOACTIVITY (Q_s = 0) AND SCATTER FRACTION (SF_{avg}) = 0.4

System type	Defect diameter (cm)	Location: C = central P = peripheral	Uptake ratio $(Q_s - Q_b)/Q_b$	Contrast factor* CF_{avg}	Scatter factor $(1 + SF_{avg})^{-1}$	Superposition D/L	Attenuation factor	Estimated contrast
Conventional	1.5	C	−1.0	0.8	0.7	0.14	0.7	−0.05
SPECT	1.5	C	−1.0	0.5	0.7	—	—	−0.35
Conventional	1.5	P	−1.0	0.8	0.7	0.14	1.4	−0.11
SPECT	1.5	P	−1.0	0.5	0.7	—	—	−0.35
Conventional	1	C	−1.0	0.5	0.7	0.16	0.8	−0.04
SPECT	1	C	−1.0	0.3	0.7	—	—	−0.21
Conventional	1	P	−1.0	0.5	0.7	0.16	1.3	−0.07
SPECT	1	P	−1.0	0.3	0.7	—	—	−0.21

* Estimated values for spatial resolution (FWHM) for conventional and SPECT were 0.9 and 1.3 cm, respectively.

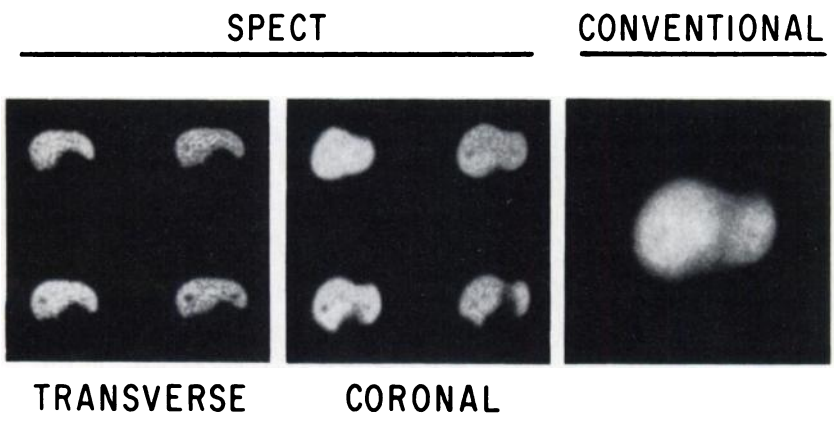

FIG. 2. Single-photon emission computed tomography (SPECT) and conventional nuclear medicine images of liver phantom containing centrally located defects. Support rods (6 mm o.d.) are visualized in coronal section containing focal regions of no radioactivity.

nation of superposition degradation with SPECT results in a significant increase in lesion contrast during imaging of small photon-deficient areas within a relatively uniform background.

A first requirement for the detection of small (resolution-sized) regions of no radioactivity is that the signal-to-noise ratio be greater than some factor k. A value of k between 4 and 5 is required in order to keep false positives and false negatives adequately scarce (*4*).

For the SPECT imaging of simple uniform sources, it is possible to compute the fractional rms noise in the reconstructed transaxial section image as a function of the total counts acquired, the dimension of the source, and the physical characteristics of the SPECT system (*3*).

Such a calculation does not adequately describe the fractional rms noise of the more complicated source distribution of the simulated liver phantom. An experimental approach was therefore used to determine whether the number of events typically acquired during a patient study for conventional and SPECT images (using dual LFOV scintillation detectors) would be adequate to detect the small regions of no radioactivity reliably.

The images (Figs. 2 and 3), together with the measured lesion contrasts (Table 2), are generally in agreement with the image contrasts (Table 1) estimated using the equations derived from the theoretical analyses of the two systems. The observed differences probably result from errors in the estimated parameter values. The photon-deficient regions were not reliably visualized with conventional imaging, whereas they were visible using SPECT.

The simulated liver phantom containing the 1- and 1.5-cm defects was also imaged with conventional incomplete-angular-sampling tomography (focal-plane or blurring type). The scans were interpreted as completely normal for both the centrally and peripherally located defect cases.

DISCUSSION

In comparing the performance of SPECT and conventional systems it might be felt that the better performance of the SPECT system results from the computer image processing involved, and that simple contrast-enhancement algorithms or display windowing would make the conventional images competitive with the SPECT images. We believe that for equal patient study times this is not true. A six-view conventional study, which we typically use, including time for patient positioning, would require about the same 26 min that the SPECT scan required in this investigation. In our example this resulted in the same total counts per slice

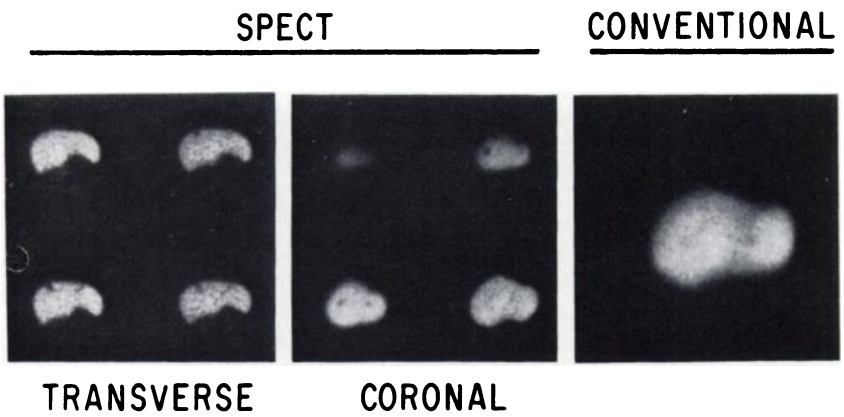

FIG. 3. SPECT and conventional nuclear medicine images of liver phantom containing peripherally located photon-deficient regions.

TABLE 2. MEASURED IMAGE CONTRASTS

Defect diameter (cm)	Location: C = central P = peripheral	Image contrast		
		SPECT (transverse)*	SPECT (coronal)†	Conventional
1.0	C	0.34	0.31	<0.08
1.5	C	0.38	0.29	<0.08
1.0	P	0.32	0.26	<0.08
1.5	P	0.54	0.47	<0.08

* Slice thickness: 6.4 mm.
† Slice thickness: 12.8 mm.

(for a complete set of 180 projections) in the SPECT image set as in a single view of the conventional image set. Use of different slice thicknesses for the SPECT images would of course change this. This appears to be a proper approach from a clinical point of view. An alternative comparison might be to require the total SPECT acquisition time for the complete set of transaxial slices to equal the total conventional acquisition time for a single view. We have previously shown that for a 2-cm area of increased uptake centrally located within a ring phantom (simulating a brain scan), the lesion is visualized in a SPECT scan containing 400,000 total counts for the complete set of transaxial slices (14,000 counts per slice), whereas it is not reliably detected with even 10 million counts in the conventional image (*3*). Of course, the % rms noise is considerably higher for the SPECT image, but the increased image contrast [Eq. (6)] for the SPECT scan results in lesion visualization since the two necessary conditions [Eqs. (2) and (3)] are simultaneously satisfied. For the conventional scan of a hot lesion, the statistical condition [Eq. (2)] is satisfied, but the lesion is not readily visualized because the image contrast, C_{image} [Eq. (5)], is below the visual threshold of the observer [Eq. (3)].

Note that windowing the conventional image, or use of contrast enhancement techniques such as background subtraction, risks increasing the false-positive rate by enhancing normal anatomical variations (positive or negative uptakes) resulting from normal variation in the thickness of the organ. A complete analysis of this aspect would require a detailed investigation using receiver operator characteristic (ROC) methods, which is beyond the scope of the present study. Furthermore, similar image-enhancing techniques would also have to be applied to the SPECT images to provide a fair comparison.

The SPECT images have been processed using a spatial reconstruction filter that does not degrade spatial resolution, so that the SPECT image contrast for the small (resolution-sized) lesions is not reduced. The conventional images have been processed only by using a digital matrix (128 × 128) during acquisition. The noise spectral density function is not identical in the two modalities, but additional processing of the conventional images—in the form of a smoothing algorithm to reduce its total noise power—would not increase visualization, since this would result in a decrease in image contrast (Tables 1 and 2) that is already at or below the threshold of visualization [Eq. (3)].

With conventional gamma-camera imaging, a major cause of lesion (increased or decreased activity) contrast degradation is the superposition of overlying and underlying radionuclide distributions (Figs. 2–4). For centrally located defects, the effect of photon attenuation

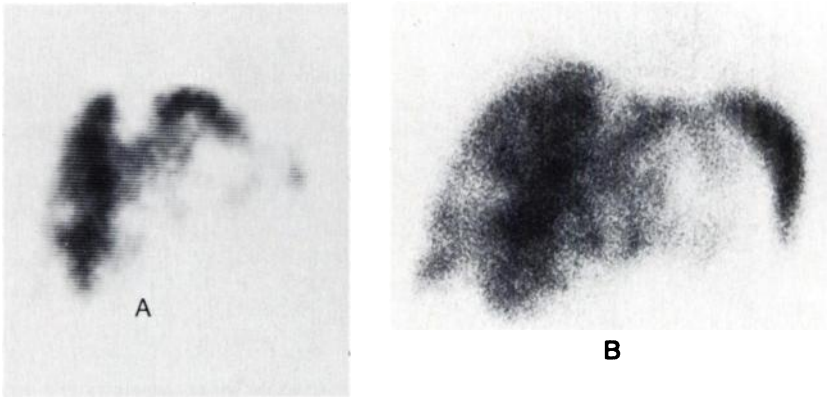

FIG. 4. A: anteriorly located coronal reconstruction (slice thickness 1.3 cm) of SPECT Tc-99m sulfur colloid liver-spleen study demonstrating multiple focal defects in liver of patient with metastatic disease. Reconstructed transaxial images (slice thickness 1.3 cm) contained approximately one million counts per slice. B: anterior gamma-camera image (containing one million counts) of same liver, with multiple focal defects seen in right and left lobes. Increased image contrast in SPECT study is demonstrated.

degrades lesion contrast by decreasing the effective signal relative to the surrounding background activity. For peripheral defects the background activity is decreased relative to the signal, and the resulting attenuation factor is greater than unity. Conventional imaging of a patient's torso typically improves the system's spatial resolution as compared with camera-based SPECT systems using a circular orbit. The effect of Compton-scattered photons on lesion contrast is comparable in the two imaging modalities. However, appropriately acquired and reconstructed SPECT images (Figs. 2–4) are essentially independent of superposition (except for partial volume effects) and, at least to a first approximation, are independent of photon attenuation, thus providing a significant increase in lesion contrast. A sufficient number of detected events must be acquired to obtain an adequate signal-to-noise ratio.

FOOTNOTES

* Siemens Gammasonics, Inc., 2000 Nuclear Drive, Des Plaines, IL 60018.

† Perkin-Elmer, Inc., 2 Crescent Place, Oceanport, NJ 07757.

ACKNOWLEDGMENTS

We are grateful for the support provided by Siemens Gammasonics, Inc. We also thank Mr. Kim Greer especially for his valuable technical assistance. Rose Boyd, Connie Faison, and Carol Bryant have provided excellent secretarial support in the preparation of the manuscript. Dr. Jaszczak is the recipient of a Senior Fellowship awarded by the National Institute of Health.

REFERENCES

1. WHITEHEAD FR: Quantitative analysis of minimum detectable lesion-to-background uptake ratios for nuclear medicine imaging systems. In *Medical Radionuclide Imaging.* Vol I. Vienna, IAEA, 1977, pp 409–434
2. SHOSA D, KAUFMAN L: Methods for evaluation of diagnostic imaging instrumentation. *Phys Med Biol* 26:101–112, 1981
3. JASZCZAK RJ, COLEMAN RE, WHITEHEAD FR: Physical factors affecting quantitative measurements using camera-based single photon emission computed tomography (SPECT). *IEEE Trans Nucl Sci* NS-28:69–80, 1981
4. WHITEHEAD FR: Minimum detectable gray-scale differences in nuclear medicine images. *J Nucl Med* 19:87–93, 1978
5. BECK RN, SCHUH MW, COHEN TD, et al: Effects of scattered radiation on scintillation detector response. In *Medical Radioisotope Scintigraphy.* Vol I. Vienna, IAEA, 1969, pp 595–616
6. DRESSER MM, KNOLL GF: Results of scattering in radioisotope imaging. *IEEE Trans Nucl Sci* NS-20:266–272, 1973
7. JASZCZAK RJ, CHANG LT, STEIN NA, et al: Whole-body single-photon emission computed tomography using dual, large-field-of-view scintillation cameras. *Phys Med Biol* 24:1123–1143, 1979
8. JASZCZAK RJ, COLEMAN RE, LIM CB: SPECT: Single photon emission computed tomography. *IEEE Trans Nucl Sci* NS-27:1137–1153, 1980
9. CHANG LT: A method for attenuation correction in radionuclide computed tomography. *IEEE Trans Nucl Sci* NS-25:638–643, 1978
10. JASZCZAK RJ, COLEMAN RE: Selected processing techniques for scintillation camera based SPECT systems. In *Single Photon Emission Computed Tomography and Other Selected Computer Topics.* JA Sorenson, Ed. New York, Society of Nuclear Medicine, 1980, pp 45–59